



**HAL**  
open science

# Acoustic monitoring of timber structures: Influence of wood species under bending loading

Marianne Perrin, Imen Yahyaoui, Xiaojing Gong

## ► To cite this version:

Marianne Perrin, Imen Yahyaoui, Xiaojing Gong. Acoustic monitoring of timber structures: Influence of wood species under bending loading. *Construction and Building Materials*, 2019, 208, pp.125-134. 10.1016/j.conbuildmat.2019.02.175 . hal-02123152

**HAL Id: hal-02123152**

**<https://hal.science/hal-02123152>**

Submitted on 22 Oct 2021

**HAL** is a multi-disciplinary open access archive for the deposit and dissemination of scientific research documents, whether they are published or not. The documents may come from teaching and research institutions in France or abroad, or from public or private research centers.

L'archive ouverte pluridisciplinaire **HAL**, est destinée au dépôt et à la diffusion de documents scientifiques de niveau recherche, publiés ou non, émanant des établissements d'enseignement et de recherche français ou étrangers, des laboratoires publics ou privés.



Distributed under a Creative Commons Attribution - NonCommercial 4.0 International License

# 1 **Acoustic monitoring of timber structures: influence of wood** 2 **species under bending loading**

3 Marianne Perrin<sup>1\*</sup>, Imen Yahyaoui<sup>1</sup>, Xiaojing Gong<sup>1</sup>

4 <sup>1</sup>Institut Clément Ader (ICA), Université de Toulouse, CNRS UMR 5312, 1 rue Lautréamont, 65000  
5 Tarbes, France

6 \*e-mail: marianne.perrin@iut-tarbes.fr (corresponding author)

7 Declarations of interest: none

## 8 **Abstract**

9 The use of wood in civil engineering structures, such as timber bridges, has been increasing in recent  
10 years. Unfortunately, our knowledge of their behaviour towards sustainability problems is far from  
11 complete and it is necessary to develop monitoring techniques like acoustic Emission (AE) that allow  
12 early identification of pathologies. This study focuses on the analysis of the influence of wood species  
13 on the acoustic response under bending loading. *The results of this experimental study show a*  
14 *correlation between AE signal features and certain failure mechanisms but also that these acoustic*  
15 *signatures are different for each timber species.*

16 **Keywords:** Timber structures, Acoustic Emission monitoring, Damage acoustic signature, Structural  
17 Health Assessment

## 18 **1. Introduction**

19 Today, the use of wood is becoming more and more widespread in the field of construction [1]. Wood  
20 is a renewable resource with low energy consumption that traps CO<sub>2</sub> during the life of the structure.  
21 Although the use of wood is an ecological solution, the integration of this material into structures  
22 remains limited because of its complex behaviour (strong anisotropy, heterogeneity, sensitivity to  
23 variations of humidity and temperature, limited mechanical properties, etc.). In order to overcome  
24 these limitations, hybrid structures have been developed in recent decades. In this context, timber-  
25 concrete bridges have been built in France. Examples include the Vallon bridge at Riou de Lantosque,  
26 the bridge of Cognin, and the bridge at Lure [1]. In addition, the European project NR2C (New Road  
27 Construction Concept), devoted to the bridges of the future, has demonstrated the mechanical interest

28 of new wood / concrete / composite decks [2]. These multi-material wood-based structures are both  
29 original and mechanically promising but the fact that this type of construction is still recent can result  
30 in some misunderstanding of their mechanical behaviour [3].

31 As a safety measure and to be able to anticipate and optimize the maintenance operations of these  
32 structures, it is interesting to detect and identify the severity of damage from its initiation. In this  
33 context, it is necessary to use a non-destructive test method to evaluate and assess the health of a  
34 structure and to predict the evolution of the damage. Acoustic emission (AE) seems an interesting  
35 technique for this purpose since it allows the response of the structure to mechanical or environmental  
36 constraints to be followed continuously. In addition, AE also enables early detection of evolving  
37 defects and the localization of acoustic sources as well as the characterization and identification of  
38 various mechanisms of damage [4]. Although the characterization of the damage mechanisms of  
39 composite materials or cementitious materials by AE is now widely reported [5], [6], [7], [8], few  
40 studies have concerned wood material. Most of the work identified in the literature shows that the  
41 anatomical structure of wood has a significant influence on its acoustic response under mechanical  
42 loadings [9], [10], [11], and Chen [12] also observed that the acoustic activity rate was proportional to  
43 the damage rate of wood. More recent work has partially correlated acoustic signatures to a particular  
44 kind of damage [13], [14], [15]. These works are generally limited to a specific wood species  
45 subjected to a particular type of stress and the assignment of acoustic signatures is often based on  
46 hypotheses.

47 The research work we present here focuses on the influence of the wood species on the acoustic  
48 response of wood material. In order to work on one of the most frequent stresses identified on timber  
49 structures [16], only the bending stress is considered. First, we will focus on the evolution of damage  
50 at different stages of loading through a conventional analysis of acoustic activity. Then we will  
51 identify the acoustic signature of the different damage mechanisms for the three species through a  
52 multi-variable analysis coupled with video tracking. The evolution of diagnostic methods and signal  
53 processing algorithms, coupled with the cross-use of several control techniques, makes it possible to  
54 increase the robustness and richness of the acoustic data. In addition to an easier correlation between  
55 the mechanisms of damage and the acoustic signatures, these developments give a better

56 understanding of the damage scenarios and the parameters influencing them, which will allow us to  
57 establish a comparison of the acoustic responses among individual species.

58

## 59 **2. Materials and testing methods**

### 60 2.1. Wood species

61 Four-point bending tests were carried out on 3 different species: two softwoods, Douglas fir  
62 (*Pseudotsuga Menziesii*) and Silver fir (*Abies Pectinata*), and a hardwood species, Poplar (*Populus*  
63 *Negra*). For the three species, the tests were performed on samples cut from the same board to limit the  
64 impact of inter-species heterogeneity and 5 samples were tested for each species. All species of wood  
65 are characterized by a heterogeneous structure and different properties in the longitudinal (L), radial  
66 (R) and tangential (T) directions [17]. Douglas fir was chosen because it is currently the species most  
67 commonly used in construction thanks to its remarkable mechanical characteristics and its natural  
68 durability properties. One of the peculiarities of Douglas fir is that its growth rings are very apparent,  
69 as the Late Wood (LW) is much denser and more colourful than the Early Wood (EW) [16] (Table 1).  
70 The second species selected was Silver fir, another resinous species, which has the particularity of  
71 being a very abundant local species in the south-west of France and which is not sufficiently  
72 developed today from a commercial point of view. Its structure and heterogeneity are different from  
73 those of Douglas fir. For example, the Silver fir has much less marked annual rings. This results in  
74 properties between the EW and the LW closer than for the Douglas fir (Table 1). The third species was  
75 Poplar, a hardwood species. Its structure is much more homogeneous for a density relatively close to  
76 that of the other two (Table 1). Thus, we can compare the behaviour of a homogeneous hardwood  
77 species with the behaviour of two heterogeneous softwood species, these three species having  
78 comparable density.

79 Table 1. Raw density of the species tested in this study (average of 5 samples), characteristics of LW  
80 et EW [18] of the species.

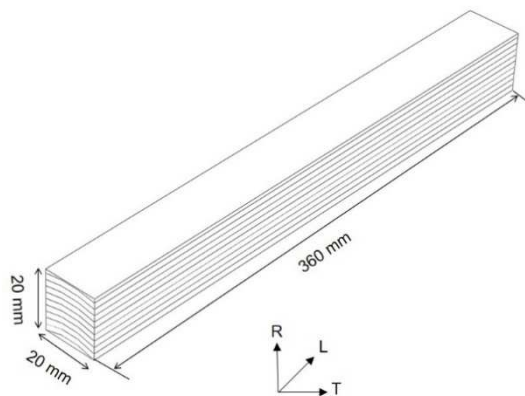
Species	Raw density in kg/m <sup>3</sup> (variability)	Density		Young Modulus (GPa)	
		EW	LW	EW	LW
Douglas fir	498.6 (±6.3%)	0.29	0.82	18.24	45.51
Silver fir	424.3 (±8.2%)	0.27	0.62	20.50	28.25
Poplar	408.1 (±2.7%)	0.4	0.48	-	-

81

82  
83  
84

## 2.2. Mechanical four-point bending test

85 The tests conducted and monitored by AE were based on standardized tests (NF B- 51-008 [19]). All  
86 of them were performed on an **MTS 20/M** electromechanical testing machine with a maximum  
87 capacity of 100 kN. Before each test, the specimens used were conditioned in a climatic chamber at 20  
88 °C and 65% relative humidity (NF B51-002 [20]) until mass stabilization. The dimensions of the  
89 specimens were 360 mm (L) x 20 mm (R) x 20 mm (T) (Figure 1).

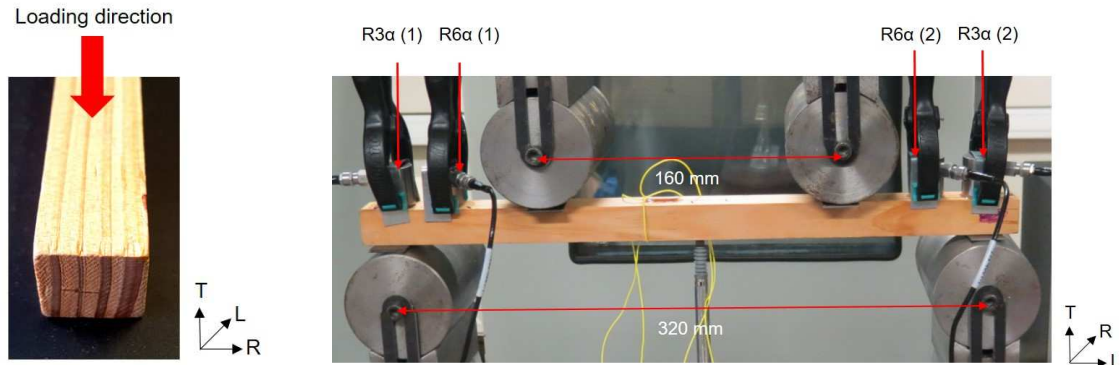


90  
91  
92  
93

Figure 1: Bending test specimen dimensions according standard NF B 51-008[19]

94 In order to ensure that the Early Wood and the Late Wood are loaded in the same way, the standard  
95 NF B 51-008 [19] requires a load to be applied parallel to the annual rings (Figure 2a). The bending  
96 tests were also carried out in imposed displacement mode, using a speed of 4 mm / min in accordance  
97 with NF B 51-008 [19]. It should be noted that a steel wedge was positioned between the supports and  
98 the sample in order to limit local indentation (Figure 2b).

99 Each test was tracked by AE and video tracking using a Canon PowerShot SX40 HS camera, **with a**  
100 **sampling rate of 24 frames per second and a resolution of 1920\*1080 pixels.**



(a)

(b)

Figure 2: Four-point bending test procedure (a) Loading direction (b) Sensor positions.

101  
102  
103  
104  
105  
106  
107

### 2.3. AE instrumentation

108 The choice of instrumentation is essential in AE. Most studies use sensor ranges having resonant  
 109 frequencies that are typically between 150 kHz and 450 kHz [9], [10], [14], [15], [21], [22], [23].  
 110 However, wood is a very dispersive material, particularly because of its heterogeneity. The  
 111 propagation of acoustic waves within the wood material is accompanied by large attenuation, which  
 112 can reach 1 dB / cm [23], [24], [25]. It is thus necessary to select a sensor that collects the maximum  
 113 of signals during the damaging of the wood material. Several authors have shown that the signals  
 114 emitted in the wood are of rather low frequency [21]. A previous study, published in TAMAP [26],  
 115 shows that the frequencies emitted during mechanical tests are lower than 100 kHz. In order to cover  
 116 the entire frequency range identified, the different tests were instrumented via two types of sensors:  
 117 R6 $\alpha$  and R3 $\alpha$  (MISTRAS Group), which have resonance frequencies of 60 kHz and 30 kHz,  
 118 respectively. The coupling of the sensors on the specimen is performed via a silicone grease and their  
 119 fixation is guaranteed by the use of metal brackets and clamps (Figure 2b). The coupling is then  
 120 checked by Hsu-Nielsen tests [27]. Each sensor was connected to a 40 dB pre-amplifier and then  
 121 connected to the acquisition system (PCI8 board from MISTRAS Group). Concerning the positioning  
 122 of the sensors, following a series of preliminary tests and in order to continue to determine the location  
 123 of the acoustic events for as long as possible during the tests, the R6 $\alpha$  and R3 $\alpha$  sensors were placed on  
 124 the top of the test piece (Figure 2b). The fact that the main damage occurs on the side under tensile

125 load of the specimen would have implied a very rapid loss of location if the sensors had been placed  
126 below the test piece. The precise position of the sensors is shown in Figure 2b.

#### 127 2.4. Tuning the acquisition parameters

128 The acquisition threshold of the system was chosen according to the signal-to-noise ratio. It was set at  
129 35 dB for all tests. Analogue filters were used to eliminate unwanted mechanical noise: high pass  
130 filter: 20 kHz, low pass filter: 400 kHz. In addition, following the preliminary tests, the values chosen  
131 for the time windows in order to identify the individual acoustic hits correctly were: **Peak Definition**  
132 **Time: 40  $\mu$ s, Hit Definition Time: 200  $\mu$ s, Hit Lockout Time: 300  $\mu$ s.**

#### 133 2.5. Statistical treatment of data

134 The AE signals were then analysed using an Unsupervised Pattern Recognition (UPR) technique with  
135 the NOESIS software (Enviroacoustics SA) to group signals with a similar acoustic signature. This  
136 type of statistical analysis is widely described in the literature [28], [29]. In this study we kept the  
137 maximum of AE features in order to obtain the most robust signal classification possible. These  
138 parameters were: rise time, counts, counts to peak, absolute energy, duration, amplitude, average  
139 frequency, frequency centroid, initiation frequency, reverberation frequency, and peak frequency.  
140 Naturally, in order to limit the weight of certain parameters in the analysis, a normalization of the data  
141 between 0 and 1 was carried out. After a comparative study of the various classification algorithms at  
142 our disposal, the k-means algorithm was used to classify the signals into different groups. The number  
143 of groups was validated through 2 statistical criteria: the Davies & Bouldin (D&B) coefficient [28]  
144 and the Tou coefficient [30].

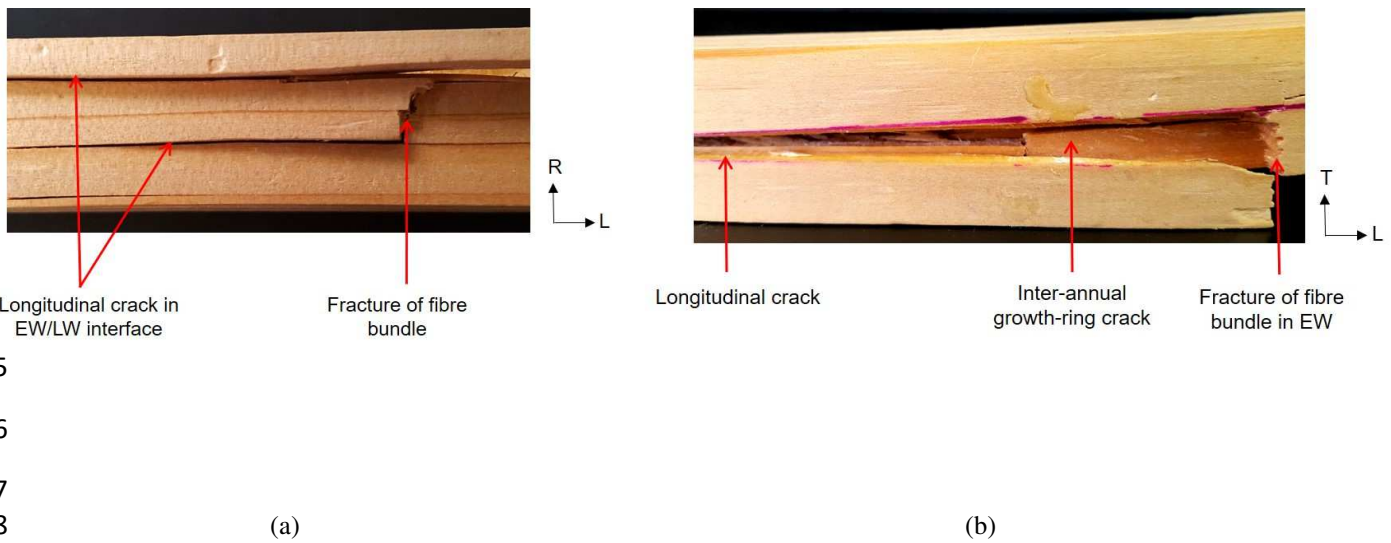
145

### 146 **3. Results and discussion**

#### 147 3.1. Bending tests on Douglas fir

148 The five specimens of Douglas fir responded similarly to the bending tests. Failure surfaces showed a  
 149 simple tensile fracture mode [31], [32]. The results presented here are those of a specimen  
 150 representative of the general behaviour observed on the batch of specimens (Figure 3). The fracture  
 151 surfaces showed numerous cracks at the EW/LW interfaces (Figure 3a) as well as large areas of  
 152 longitudinal cracks (Figure 3b). The detachment of one or more initial wood bundles was also widely  
 153 observed (Figure 3b) (one bundle corresponds to all the fibres of one or more growth rings).

154



160 Figure 3: Observations of the Douglas fir specimen (a) tension face (LR view)  
 161 (b) Side view (TL view)

162

164 Images from the video permitted visual and audio analysis of the damage during the bending test.  
 165 Many audible noises (unaccompanied by visible damage) could be identified at specific times during  
 166 the test, as well as some macroscopic damage. Table 2 presents the significant moments.

167

168 Table 2: Record of feature points on video recording.  
 169

Hit number (Figure 5)	Time (s)	Observation/listening
1	131.5	Audible noise (no visible damage)
2	147.8	Audible noise (no visible damage)
3	152.6	Audible noise with macroscopic rupture (Figure 4 a)
4	154	Audible noise with macroscopic rupture (Figure 4b)
5	159.2	Audible noise (no visible damage)

170

171 Figure 4 shows the two instances of macroscopic damage observed during the test.

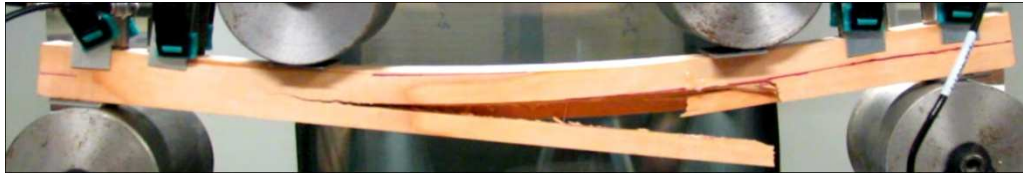
172



173

174

(a)



175

176

(b)

Figure 4: (a) First macroscopic fracture (b) second macroscopic fracture

178

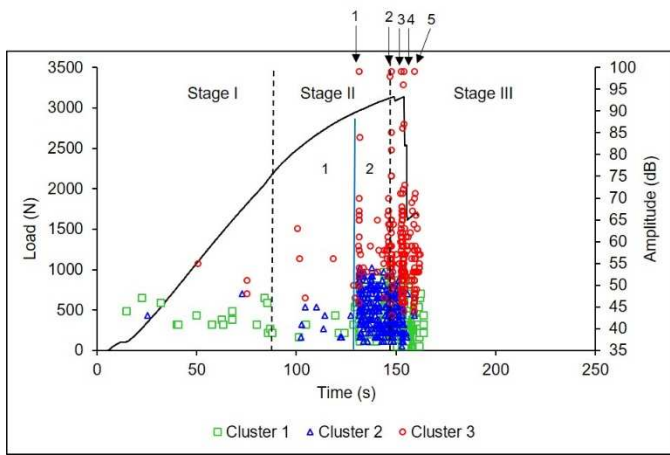
179 These two occurrences of macroscopic damage were generated by the zones of cracking between the  
180 different rings, and also by the breaking of bundles of fibres and the propagation of cracks in the  
181 longitudinal direction. The pull-out of a bundle of fibres, as during damage occurrences 3 and 4, was a  
182 brutal mechanism (fibre breakage then crack propagation).

183 These characteristic moments were also identified on the recording of the associated acoustic activity.  
184 Figure 5a shows this activity collected on the sensor that recorded the most hits. Three distinct stages  
185 can be observed. The first stage corresponds to the linear part of the Load-time curve. It is  
186 characterized by the detection of acoustic signals of amplitude not exceeding 55 dB. The second stage  
187 begins when the Load-time curve begins to become non-linear and ends at the point where the load is  
188 highest. In terms of acoustic response, this stage can be divided into two parts. During Part 1, the  
189 acoustic activity undergoes a small increase and the amplitude does not exceed 65 dB. Part 2 starts at  $t$   
190  $= 131.5$ s with an audible noise. It is characterized by an increase in the number of hits together with  
191 the recording of high amplitude signals (99 dB). The third stage corresponds to the rupture stage. In  
192 terms of acoustic response, the number of hits continues to increase very significantly. The  
193 multiplicity of sources of acoustic emission appears clearly in Figure 5a, where a very broad spectrum  
194 of amplitudes, ranging from 35 dB to 99 dB, is observed.

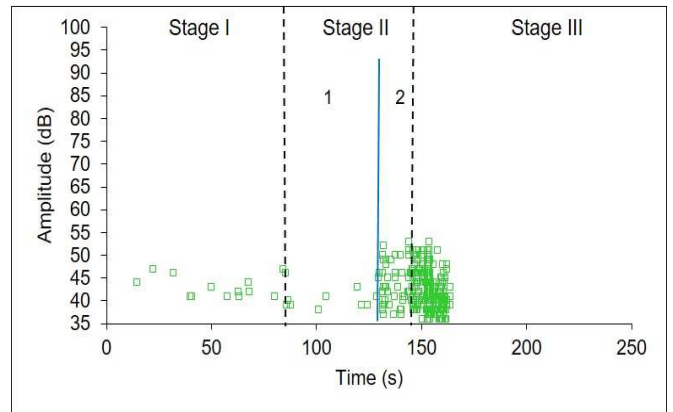
195 The statistical classification of the signals, based on the k-means algorithm and validated by the  
196 coefficients of Davies & Bouldin and Tou, presented 3 clusters of significantly different signals. The  
197 first cluster (Figure 5b) contained 44% of the signals. This cluster appeared early during the test then

198 intensified from 148.7 s, when a peak load was recorded. In addition, cluster 1 was clearly visible at  
 199 the time of the two macroscopic breaks. The second cluster (Figure 5c) contained 35% of the signals.  
 200 Few signals appeared before 131.5 s. Then the appearance of this cluster of signals intensified. It  
 201 should be noted that the increase in the activity density of the second cluster was consecutive to the  
 202 first audible signal at 99 dB. This cluster of signals also ended early compared with the other two  
 203 clusters. The third cluster (Figure 5d) included 21% of the signals and started to appear significantly as  
 204 audible noises began to be emitted (131.5s).

205



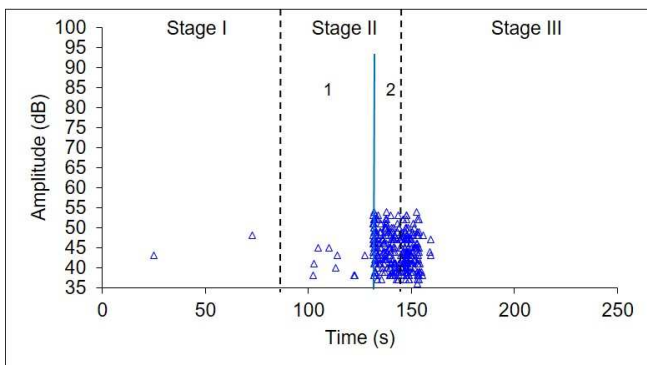
206



207

(a)

(b)



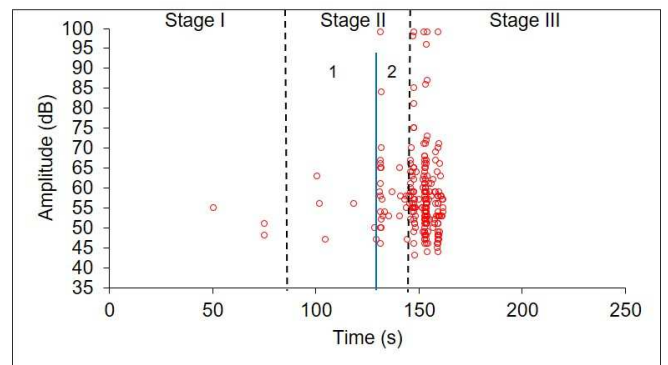
208

209

210

(c)

(d)



211 *Figure 5: AE activity for the Douglas fir specimen during the 4 point bending test, (a) evolution of signal*  
 212 *amplitude and load (b) cluster 1, (c) cluster 2 (d) cluster 3*

213

214

215 Following the analysis of the video data and the associated acoustic activity, a damage scenario was  
216 developed, allowing each signal cluster to be associated with a specific damage mechanism. From the  
217 beginning of the first audible noises at  $t = 131.5$  s, the acoustic activity increased, in particular in the  
218 second cluster of signals. High amplitude (99 dB) signals were synchronized with audible breakage  
219 sounds. This means that, from  $t = 131.5$  s, wood fibres started to break. Following these first breaks,  
220 mobility mechanisms were set up in the shear planes, leading to cracks between the EW/LW rings.  
221 Thus, from 131.5 s, a significant amplification of the second cluster of signals was observed. The  
222 evolution of the damage resulted in breakage of wood bundles for  $t = 152.6$  s and  $t = 154$  s,  
223 accompanied by a significant increase in the first and third clusters of signals. This macroscopic  
224 damage was the consequence of fibre breaks in the tensile zone being transformed into longitudinal  
225 propagation when a singularity was encountered in the specimen. This damage scenario based on  
226 visual observations correlated with the acoustic activity made it possible to label the three clusters of  
227 signals. The first cluster was associated with the macroscopic failure mechanisms observed at 152.6 s  
228 and 154 s. These signals were related to the coalescence and propagation of longitudinal microcracks  
229 at the beginning of the test and then to the longitudinal propagation of macroscopic cracks in stage III.  
230 The second cluster of signals corresponded to the inter-laminar shear mechanisms at the EW / LW  
231 interfaces. These mechanisms created signals of low amplitude and low energy. The most energetic  
232 signals (cluster 3) were synchronized with the audible sounds of fibre breaks and thus ultimately  
233 associated with breaks in fibre bundles.

234

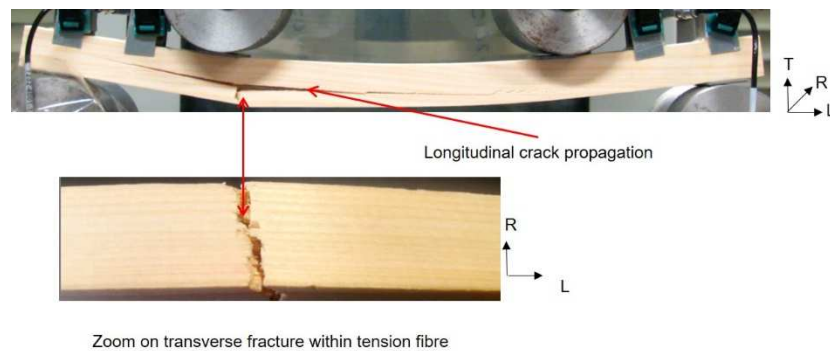
### 235 3.2. Bending tests on Silver fir

236 The mechanical response of the five test pieces of Silver fir to the bending stresses was similar to  
237 that of the Douglas fir but the ruptures observed on the specimens of Silver fir were sudden with little  
238 prior warning. The final rupture of the specimen began in the tension region by the propagation of a  
239 transverse crack in mode I (opening crack), followed by a longitudinal propagation in modes I + II  
240 (opening and shearing crack) until the final failure (Figure 6).

241

242

243



244

Figure 6: Fracture surfaces observed on Silver fir specimen.

245

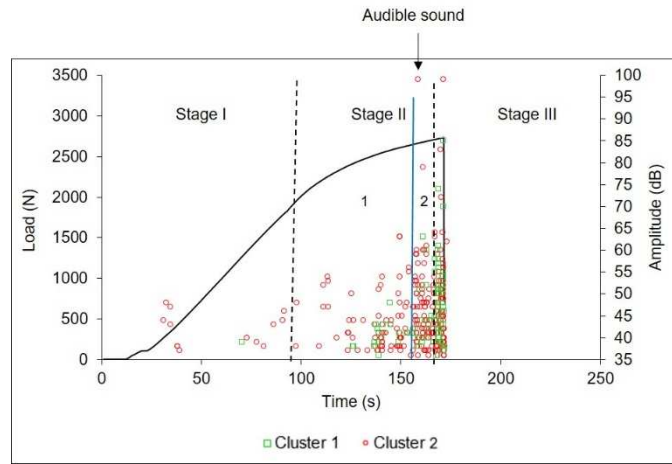
246

247 The video follow-up showed no precursors to the failure of the specimen, except a fibre rupture noise  
248 at  $t = 158.6s$ . As in the Douglas fir bending tests, the acoustic activity collected on the Silver fir  
249 presented three different stages. The number of hits cumulated in the first stage evolved in a regular  
250 manner (Figure 7a). The amplitude of recorded signals did not exceed 50 dB. In terms of acoustic  
251 response, the second stage could be divided into two parts according to the acoustic activity rate  
252 recorded. Amplitudes in stage II-1 did not exceed 65 dB (Figure 7a). Stage II-2 began with the  
253 recording of a high amplitude signal (99 dB) at  $t = 158.6s$ . The last stage was almost instantaneous. At  
254 the acoustic response level at this time, the hit amplitude (Figure 7a) covered the entire range from the  
255 lowest to the highest amplitude (from 35 dB to 99 dB). There was also a huge increase in the number  
256 of hits.

257 The ranking obtained by the k-means algorithm is presented in Figure 7. The number of signal clusters  
258 validated by the statistical criteria of Davies & Bouldin and Tou was two.

259 The first cluster (Figure 7b) contained 24% of the signals. It started relatively late in the test. There  
260 was an increase in activity at the time of the final rupture. The second cluster (Figure 7c) contained  
261 76% of the signals. The average amplitude of the signals of the second cluster was small. It was also  
262 noted that the amplitudes increased as the rupture phase approached.

263



264

265

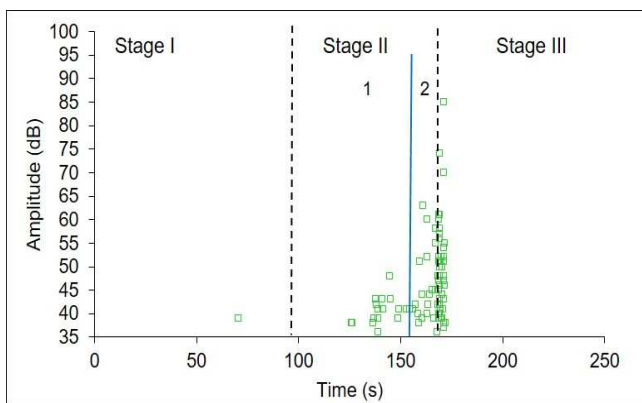
266

267

268

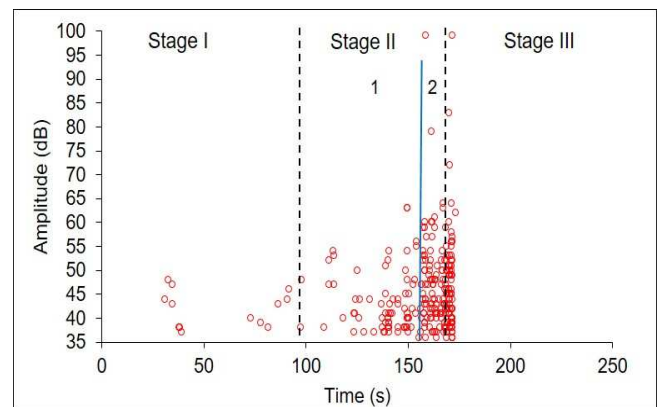
269

(a)



270

(b)



(c)

272 *Figure 7: AE activity for the Silver fir specimen during the 4 point bending test, (a) evolution of signal amplitude*  
 273 *and load (b) cluster 1, (c) cluster 2.*

274

275 To label the two clusters of signals dissociated by multi-variable statistical analysis, we mainly relied

276 on the correlation between the acoustic emission and the film record. The first cluster began in stage II

277 with coalescence and propagation of longitudinal microcracks. Then, in the rupture stage (stage III),

278 the signals of the first cluster corresponded to the propagation of the longitudinal crack in mode I + II

279 (opening and shearing crack) identifiable on the lateral face of the specimen (Figure 6). The second

280 class of signals represented a progressive phenomenon that started very early in the test. The

281 mechanism of damage present at that time was the transverse microcracking that started during stage I.  
282 The propagation and the coalescence of these transverse microcracks led to the mode I breakdown of  
283 fibres over the full width of the tensile part of the specimen. The audible noise specific to fibre breaks  
284 identified at the beginning of stage II-2 corresponded to the high amplitude signals of the second class.  
285

### 286 3.3. Bending tests on Poplar

287 Poplar specimens showed a combined failure mode (simple traction and bevel propagation) that  
288 started in the tensile zone of the specimen. The fracture surfaces presented in Figure 8 is representative  
289 of the behaviour of Poplar under bending stress. Crack initiations were located in the area of minimum  
290 stiffness lying under the top loading supports, where a zone of matting that weakened the material was  
291 observable (Figure 9). Under the effect of the bending stress, the two cracks propagated in mixed  
292 mode I + II (opening and shearing crack) crosswise towards the centre of the specimen. The fracture  
293 surfaces on the broken specimens formed a cross at (X). A major mechanism was observed on the  
294 fracture surfaces of the specimen: an inclined cracking mechanism (mix of microcracks in several  
295 planes of the sample).

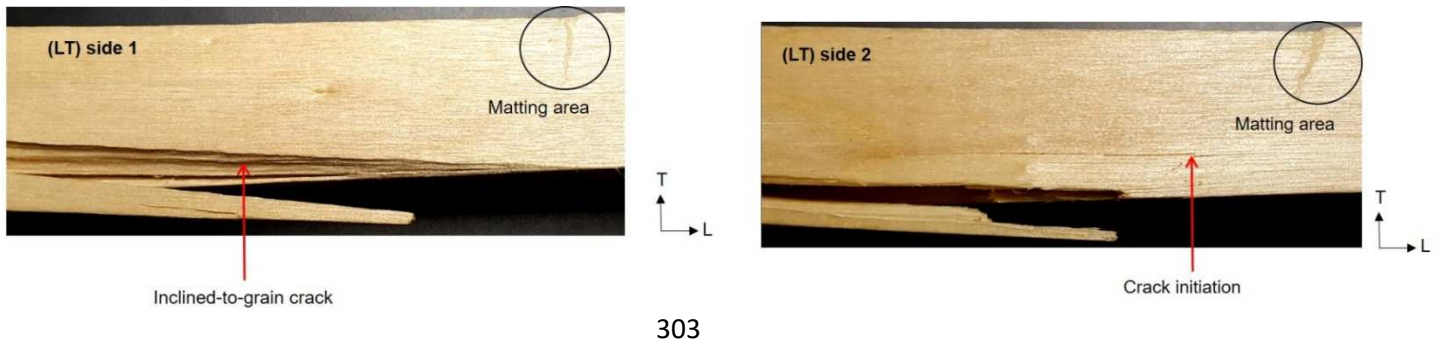


296  
297 (a)



298  
299 (b)

300  
301  
302 *Figure 8: Fracture surfaces observed on Poplar specimen (a) side view (LT view) (b) tension face (LR view).*



304

305 (a)

(b)

306

307 *Figure 9: (a) Front of the specimen (b) Rear face of the specimen.*

308 Four images corresponding to characteristic moments of the damage were extracted from the film

309 (Figure 10). Images A and B, identified at different times during the test, showed no visible damage. It

310 should be noted that image B corresponded to the moment of the first audible noise identified during

311 the test. Image C showed the presence of macroscopic damage. This was a detachment of fibres,

312 observed in the tension part of the specimen under the upper left loading support, followed by a crack

313 propagation over a short distance. This first failure was followed by two other very rapid breaks that

314 started simultaneously on the two opposite sides of the specimen (Figure 10 - image D).

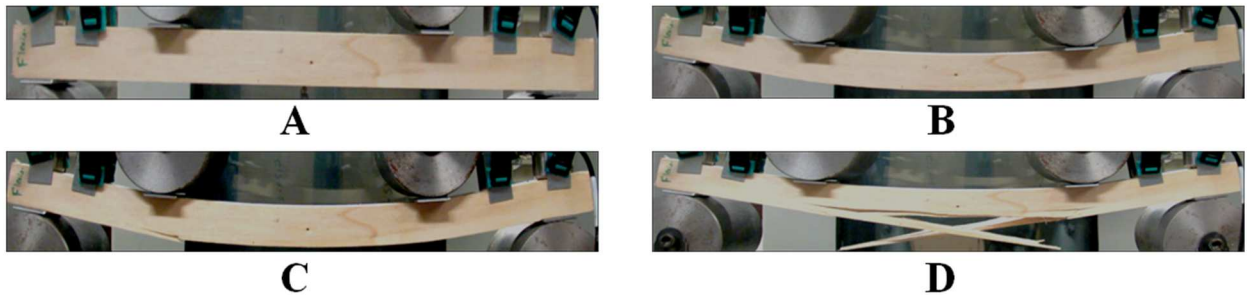


Figure 10: Characteristic images of the poplar sample damage extracted from the film.

315

316 As for the two preceding species, three specific stages could be identified on the Load-time curve.

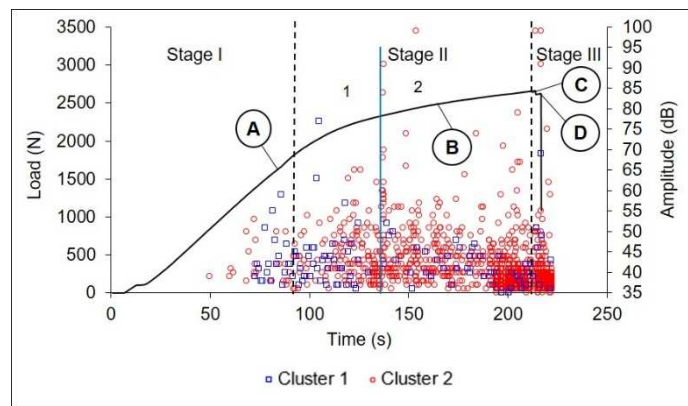
317 Recording of acoustic hits started from  $t = 50$  s. The number of cumulated hits (Figure 11a) was

318 relatively small in this stage. The amplitude of the recorded signals varied between 35 dB and 55 dB

319 (Figure 11). In terms of acoustic response, the second stage showed that the number of hits intensified

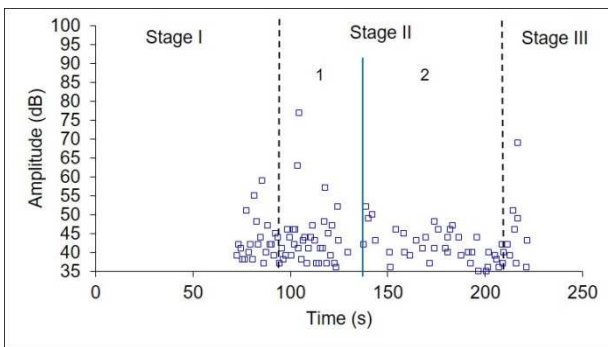
320 as the test progressed. Figure 11 reveals two distinct parts in this second stage. In stage II-1, the

321 amplitudes remained modest (<60 dB) whereas, in stage II-2, a significant increase in amplitudes  
 322 could be observed with signals exceeding 90 dB. We also noted a very significant increase in the  
 323 number of hits around 200 s. The last stage was almost instantaneous. The amplitude of the recorded  
 324 signals varied between 35 dB and 99 dB, and the number of high amplitude signals was relatively  
 325 small.  
 326 The results of the classification of acoustic signals by the k-means method are presented in Figure 11.  
 327 Two different signal clusters were identified by the **Davies&Bouldin** and Tou criteria.

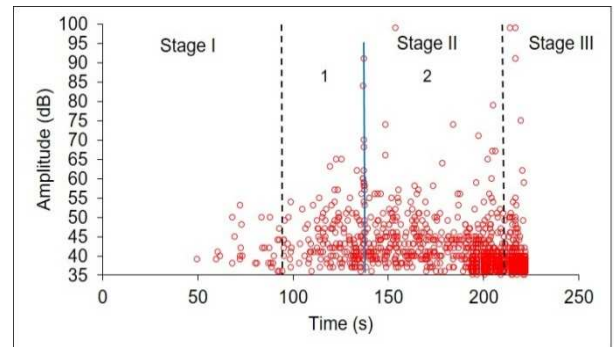


(a)

328  
 329  
 330  
 331



(b)



(c)

332  
 333  
 334  
 335  
 336  
 337  
 338

Figure 11: AE activity for the Poplar specimen during the 4-point bending test, (a) evolution of signal amplitude and load (information A, B, C and D refer to Figure 10) (b) cluster 1, (c) cluster 2.

339 Figures 11b and 11c show that the two clusters of signals evolved in particular ways. The first cluster  
 340 (Figure 11b) contained only 5% of the signals. It appeared around 70 s and showed a homogeneous  
 341 distribution of the signals throughout the test. The evolution of the second cluster of signals (Figure  
 342 11c) was much more significant. The cluster contained 95% of the signals and started at 50s. It

343 showed weak activity in stage I, a progressive intensification in stage II and very intense activity at the  
344 end of the test. It should be noted that the second cluster of signals included all the signals having high  
345 amplitudes.

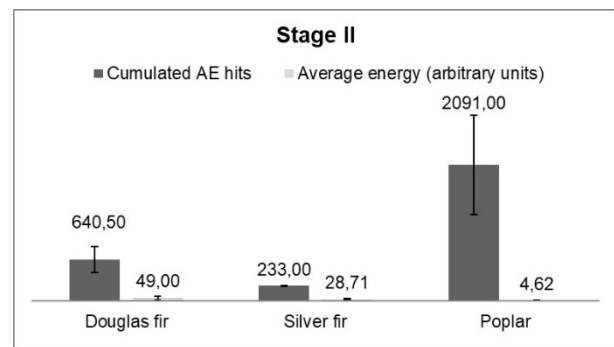
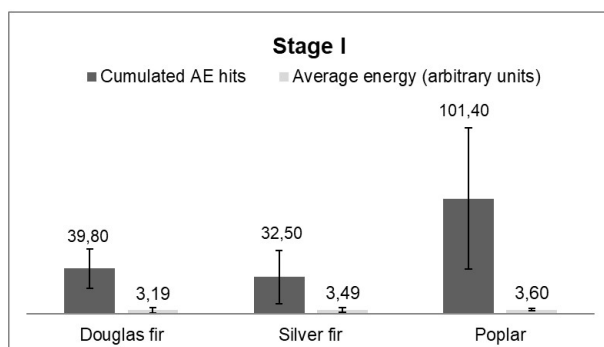
346 If we compare the observations made on the specimen and the evolution of the two clusters of signals,  
347 it would seem that the first cluster of signals can be attributed to the permanent deformation in  
348 compression obtained by the matting effect, *although we have no direct evidence* (Figure 9). This is a  
349 local shear deformation of the fibres observed on all specimens of Poplar. This deformation does not  
350 lead to any great damage, which explains why it generates only 5% of the signals. *The signals of the*  
351 *second cluster correspond to* the different types of microfissuring (longitudinal and transversal) as well  
352 as to the breaking of fibres, and this cluster includes almost all signals with disparate characteristics as  
353 shown by the variety of amplitudes. The evolution of its activity during the *test is in line* with the  
354 evolution of the damage. The signals detected during stage I *are generated* during the initiation of  
355 microcracks, the coalescence and propagation of these microcracks occur in stage II and this activity  
356 intensifies during stage II-2 as the propagation of microcracks begins to be accompanied by fibre  
357 breaks. This is confirmed in stage III, with several high amplitude signals associated with a significant  
358 acoustic activity between 35 and 50 dB. These signals come from macroscopic cracking and rupture of  
359 the specimen.

360

### 361 3.4 Comparison of acoustic responses

362 The three species of wood studied in these works, stressed in bending, exhibit clearly  
363 different behaviours with respect to their damage. One of the main reasons that can be  
364 invoked concerns their anatomical structures. Several comparisons can be made, first of all by  
365 comparing hardwood and softwood species. Several studies in the literature have shown that  
366 softwood species are more emissive than hardwood species [10], [11], [21], [33]. We show  
367 here that these results are to be taken with caution, as already found by Chen [12], since the  
368 detection sensitivity of AE is largely dependent on the choice of instrumentation and  
369 acquisition parameters. The analysis of our results indicates that the intensity of the acoustic

370 activity varies from one stage to another depending on the species. In stage I, we find that the  
 371 two softwoods (Douglas fir and Silver fir) generate an equivalent number of signals (Figure  
 372 12a). On the other hand, the Poplar generates at least three times more signals than the two  
 373 softwoods (Figure 12a). Finally, if we compare the average energy of each hit, we can see that  
 374 the AE of the Douglas fir, Poplar and Silver fir have comparable average energies. During  
 375 stage II, the Poplar emits many more signals than the two other woods (Figure 12b). On the  
 376 other hand, although the number of signals generated by the Poplar is more than three times  
 377 that generated by the Douglas fir, the average energy released by the Poplar signals is ten  
 378 times less than that generated by the Douglas fir. Regarding the Silver fir, the average energy  
 379 released is approximately half that released by the Douglas fir. In stage III, the breaking stage,  
 380 Poplar still generates lots of signals (Figure 12c). The small number of cumulated hits  
 381 generated by the Silver fir during its damage reflects its instantaneous failure. Nevertheless,  
 382 the average energy released is the largest of the three species. The average energy released by  
 383 the second softwood species is slightly lower as that released by the Silver fir. In Poplar, the  
 384 rupture stage is characterized by a large number of low energy signals.

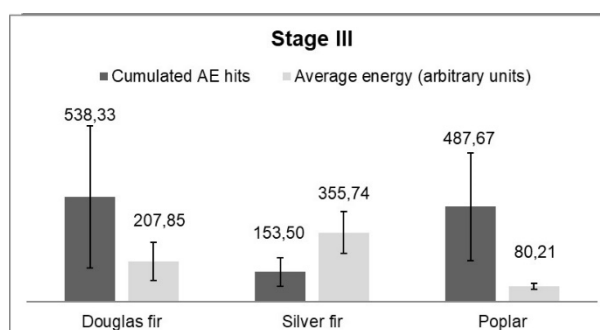


385

(a)

(b)

386



387

(c)

388

*Figure 12: Comparison of the AE response of the three wood species during the three stages of loading*

389

*(a) stage I, (b) stage II (c) stage III (AE energy =  $\int_T A. dt$ ).*

390

391 The evolution of the number of hits and the energy released reflects the behaviour of the three

392 species when they are undergoing damage. Douglas fir shows a significant increase in energy

393 released in stage II. This is related to the specific mechanisms that are set up at the interfaces

394 between EW and LW. Douglas fir is one of the species where the heterogeneity between early

395 wood and late wood is strong [18]. For the Douglas fir, the density can differ by a factor of

396 three (0.82 for LW, 0.29 for EW) [18], which causes stress concentrations at the EW / LW

397 interfaces, thus establishing complex damage mechanisms. For the Silver fir, the density

398 differs only by a factor of 2.3 (0.62 for LW, 0.27 for EW) [18]. This may explain the

399 difference in behaviour under loading of the Silver fir, where there is almost no damage

400 between growth rings. The particularity of the Silver fir is the sudden release of energy at the

401 time of the breakage phase. Concerning Poplar, the differences between EW and LW are very

402 small, as shown by the density values: 0.48 for LW and 0.40 for EW [18]. Poplar is a diffuse

403 pore wood. EW and LW vessels have almost the same diameter and are evenly distributed

404 over spring wood and summer wood. Its relative homogeneity results in damage mechanisms

405 that are initiated quickly but evolve progressively until rupture, thus generating numerous but

406 not very energetic signals. One of the consequences of this is the difficulty of drawing up a

407 detailed classification of the different types of signals coming from Poplar.

408

#### 409 **4. Conclusion**

410 The aim of this research work was to understand the differences in acoustic response

411 according to the wood species under bending stress.

412 Regarding the influence of wood species on the overall acoustic activity, we observed a  
413 different behaviour that can be summarized as follows: overall, the hardwood species emitted  
414 more signals than either of the softwood species, but the signals were of low energy. The  
415 comparison between the two softwood species also showed different behaviours. The species  
416 of Douglas fir was very emissive throughout the test while the Silver fir was characterized by  
417 a very sudden break with very energetic signals at the end of the test. The statistical  
418 classifications implemented during this study showed that three separate classes of signals  
419 could be identified for Douglas fir (cracking at EW/LW interfaces, longitudinal cracking, and  
420 fibre breakage). Only two mechanisms were observed and identified in the acoustic activity of  
421 the Silver fir: longitudinal cracking and fibre breakage. For poplar, due to its relatively  
422 homogeneous anatomical structure, the statistical processing of the data did not make it  
423 possible to discriminate the signals coming from different damage mechanisms.

424 Our results show that a comparison of the acoustic behaviour of different wood species cannot  
425 be limited to a simple analysis of the acoustic emissivity. The hardwood and softwood species  
426 studied showed different behaviours not only in the number of hits emitted but also in the  
427 energies released. On the other hand, the use of statistical processing of acoustic data coupled  
428 with video tracking showed that certain specific mechanisms were responsible for the  
429 differences in acoustic behaviour observed between species. This was the case, for example,  
430 for cracking mechanisms at the EW / LW interfaces in the case of the Douglas fir, which  
431 remains the species mainly used in the construction of wooden structures today. The  
432 recognition of damage mechanisms through the recording of specific acoustic signals opens  
433 up many interesting perspectives for the development of wood-based structures, in particular  
434 with regard to the problems of maintenance of such structures. Before arriving at this stage, it  
435 will nevertheless be necessary to be able in a short course to decorrelate the signals collected  
436 from measurement biases (propagation, natural frequency of the sensor, etc.) that modify the

437 original acoustic source. This will make it possible to identify universal acoustic signatures  
438 that are independent on the measurement systems and thus make the analysis of information  
439 reliable. it will also have to be able to solve the problem of the transition from the laboratory  
440 specimen to the actual structure. This involves solving the questions related to on-site  
441 instrumentation but also the definition of relevant indicators to alert bridges managers. Not  
442 only the experience gained on other types of structures [34], but also the improvement and the  
443 miniaturization of the sensors and the electronics will certainly be necessary in order to  
444 answer to these imperatives.

445 This research was funded by the French Ministry of Higher Education, Research and  
446 Innovation.

#### 447 **References**

- 448 [1] F. Renaudin, P. Jandin, Design of wood-concrete composite beams under deck bridge-  
449 Theoretical developments and constructions examples, 3<sup>rd</sup> International conference on Timber  
450 Bridges, Skelleftea, Sweden, 2017
- 451 [2] O. Ben Mekki, F. Toutlemonde, Experimental Validation of a 10-m-Span Composite  
452 UHPFRC–Carbon Fibers–Timber Bridge Concept, *J. Bridge Eng.*, 16(1) (2011) 148-157.  
453 [https://doi.org/10.1061/\(ASCE\)BE.1943-5592.0000114](https://doi.org/10.1061/(ASCE)BE.1943-5592.0000114).
- 454 [3] V.A. Trung Nguyen, Multi-renforcement du bois lamellé-collé – Etude théorique et  
455 expérimentale, Doctoral Dissertation, Ecole Nationale des Ponts et Chaussées, Paris, France,  
456 2010
- 457 [4] N. Godin, P. Reynaud, G. Fantozzi, Emission acoustique et durabilité des composites,  
458 ISTE Editions, 2018, ISBN : 978-1-78405-434-2
- 459 [5] K. Otsuka, H. Date, Fracture process zone in concrete tension specimen, *Eng. Fract.*  
460 *Mech.* 65 (2000)111-131. [https://doi.org/10.1016/S0013-7944\(99\)00111-3](https://doi.org/10.1016/S0013-7944(99)00111-3)
- 461 [6] V. Kostopoulos, T. Loutas, K. Dassios, Fracture behavior and damage mechanisms  
462 identification of SiC/glass ceramic composites using AE monitoring, *Compos. Sci. Technol.*  
463 67(7–8) (2007) 1740–1746. <https://doi.org/10.1016/j.compscitech.2005.02.002>
- 464 [7] J. Saliba, A. Loukili, F. Grondin, J.P. Regoin, Experimental study of creep-damage in  
465 concrete by acoustic emission technique, *Mater Struct.* 45(9) (2012) 1389-1401.  
466 <https://doi.org/10.1617/s11527-012-9840-3>
- 467 [8] V. Munoz, B. Valès, M. Perrin, M.L. Pastor, H. Weleman, A. Cantarel, M. Karama,  
468 Damage detection in CFRP by coupling acoustic emission and infrared thermography,  
469 *Composites Part B* 85 (2016) 68-75. <https://doi.org/10.1016/j.compositesb.2015.09.011>
- 470 [9] M.P. Ansell, Acoustic emission from softwoods in tension, *Wood. Sci. Technol.* 16(1)  
471 (1982) 35–57. <https://doi.org/10.1007/BF00351373>

- 472 [10] A. Vautrin, B. Harris, Acoustic emission characterization of flexural loading damage in  
473 wood, *J. Mat. Sc.* 22(10) (1987) 3707–3716. <https://doi.org/10.1007/BF01161482>
- 474 [11] A. Reiterer, S.E. Stanzl-Tschegg, E.K. Tschegg, Mode I fracture and acoustic emission  
475 of softwood and hardwood, *Wood. Sci. Technol.* 34(5) (2000) 417-430.  
476 <https://doi.org/10.1007/s002260000056>
- 477 [12] Z. Chen, B. Gabbitas, D. Hunt, Monitoring the fracture of wood in torsion using acoustic  
478 emission, *J. Mater. Sci.* 41(12) (2006) 3645–3655. <https://doi.org/10.1007/s10853-006-6292-6>
- 479 [13] F. Baensch, M. Zauner, S.J. Sanabria, M.G.R. Sause, B.R. Pinzer, A.J. Brunner, M.  
480 Stampanoni, P. Niemz, Damage evolution in wood: synchrotron radiation micro-computed  
481 tomography (SR $\mu$ CT) as complementary tool for interpreting acoustic emission (AE)  
482 behavior, *Holzforschung* 69(8) (2015) 1015-1025. <https://doi.org/10.1515/hf-2014-0152>
- 483 [14] F. Lamy, M. Takarli, N. Angellier, F. Dubois, O. Pop, Acoustic emission technique for  
484 fracture analysis in wood materials, *Int. J. Fract.* 192(1) (2015) 57-70.  
485 <https://doi.org/10.1007/s10704-014-9985-x>
- 486 [15] M. Diakhate, E. Bastidas-Arteaga, R. Moutou-Pitti, F. Schoefs, Probabilistic  
487 improvement of crack propagation monitoring by using acoustic emission, *Fracture, Fatigue,*  
488 *Failure and Damage Evolution* 8 (2017)111-118. [https://doi.org/10.1007/978-3-319-42195-](https://doi.org/10.1007/978-3-319-42195-7_16)  
489 [7\\_16](https://doi.org/10.1007/978-3-319-42195-7_16)
- 490 [16] J. Venet, R. Keller, Identification et classement des bois français, Second ed., ENGREF,  
491 Nancy, France 1987, ISBN 978-2-857-10020-1.
- 492 [17] R.J. Ross, Wood handbook : wood as an engineering material, USDA Forest Service,  
493 Forest Products Laboratory, General Technical Report FPL- GTR-190, (2010) 509,  
494 <https://doi.org/10.2737/FPL-GTR-190>
- 495 [18] F.P. Kolmann, W.A. Côté, Principles of Wood Sciences and Technology, Part I: solid  
496 wood, Springer Science&Business Media, 2012, ISBN 978-3-642-87928-9
- 497 [19] NF B51-008, Solid wood – Static bending – Determination of ultimate strength in static  
498 bending using small clear specimens, AFNOR editions, 2017
- 499 [20] NF B51-002, Standard test method for physical and mechanical characteristics of wood,  
500 AFNOR editions, 1942
- 501 [21] D. Varner, M. Cerny, M. Varner, M. Fajman, Possible sources of acoustic emission  
502 during static bending test of wood specimen, *Acta Universitatis Agriculturae Mendelianae*  
503 *Brunensis* 60(3) (2012) 199–206. <https://doi.org/10.11118/actaun201260030199>
- 504 [22] Y. Wu, Z.P. Shao, F. Wang, G.L. Tian, Acoustic emission characteristics and felicity  
505 effect of wood fracture perpendicular to the grain, *J. Trop. For. Sci.* 26 (4) (2014) 522-531.  
506 <https://www.jstor.org/stable/43150938>
- 507 [23] F. Ritschel, A.J. Brunner, P. Niemz, Nondestructive evolution of damage accumulation  
508 in tensile test specimens made from solid wood and layered wood materials, *Compo. Struct.*  
509 95 (2013) 44-52. <https://doi.org/10.1016/j.compstruct.2012.06.020>
- 510 [24] V. Bucur, Acoustics of wood, Springer Series in Wood Science, Germany, 2006, ISBN  
511 978-3-540-30594-1
- 512 [25] E.N. Landis, Acoustic Emission in Woods, in C. Grosse, M. Ohtsu (Eds), *Acoustic*  
513 *Emission Testing*, Springer-Verlag, 2008, pp. 311-322, ISBN 978-3-540-69895-1,  
514 <https://doi.org/10.1007/978-3-540-69972-9>
- 515 [26] I. Yahyaoui, M. Perrin, X.J. Gong, Damage evolution in wood under tensile loading

516 monitored by acoustic emission, TAMAP Journals of Engineering, 2017, article ID-15,  
517 [http://www.tamap.org/Content/AID\\_15-25102017161531-.pdf](http://www.tamap.org/Content/AID_15-25102017161531-.pdf)

518 [27] N. Hsu, F. Breckenridge, Characterization and calibration of acoustic emission sensors,  
519 *Materials Evaluation* 39 (1) (1981) 60-68

520 [28] S. Huguet, Application de classificateurs aux données d'émission acoustique :  
521 identification de la signature acoustique des mécanismes d'endommagement dans les  
522 composites à matrice polymère, Doctoral dissertation, INSA de Lyon, Lyon, France 2002

523 [29] A. Foulon, Détermination de la signature acoustique de la corrosion des composites SVR  
524 (stratifiés verre résine), Doctoral dissertation, Technology University of Compiègne,  
525 Compiègne, France, 2015

526 [30] JT. Tou, Dynoc – A dynamic optimal cluster-seeking technique, *International Journal of*  
527 *Parallel Programming* 8 (6) (1979) 541-547

528 [31] J. Bodig, B. Jayne, Mechanics of wood and wood composites, Krieger Publishing  
529 Company, 1993, ISBN 978-0-894-64777-2

530 [32] G. Pluinage, La rupture du bois et de ses composites, Cépaduès-Editions, 2005, ISBN  
531 978-2-85428-292-4

532 [33] S. Aicher, L. Höfflin, G. Dill-Langer, Damage evolution and acoustic emission of wood  
533 at tension perpendicular to fiber, *Holz Roh und Werks.* 59(1-2) (2001) 104–116.  
534 <https://doi.org/10.1007/s001070050482>

535 [34] M. Shigeishi, S. Colombo, K.J. Broughton, H. Rutledge, A.J. Batchelor, M.C. Forde,  
536 Acoustic emission to assess and monitor the integrity of bridges, *Construction and building*  
537 *materials* 15(1) (2001) 35-49